Journal of Power Sources 195 (2010) 1849–1853

Contents lists available at ScienceDirect

Journal of Power Sources

journal homepage: www.elsevier.com/locate/jpowsour

Short communication

A novel electrolyte for intermediate solid oxide fuel cells

Jihai Cheng[a,b,*], Weitao Bao[a], Chengliang Han[a], Wenbing Cao[a]

[a] Department of Chemistry and Materials Engineering, Hefei University, Hefei, 230022, China
[b] Key Lab of Powder and Energy Sources Materials, Hefei University, Hefei, 230022, China

ARTICLE INFO

Article history:
Received 7 October 2009
Accepted 7 October 2009
Available online 7 November 2009

Keywords:
Solid oxide fuel cells
Electrolyte
Scheelite
Sinterability
Electrochemical property

ABSTRACT

Scheelite-type, $La_xCa_{1-x}MoO_{4+\delta}$ electrolyte powders, are prepared by the sol–gel process. The crystal structure of the samples is determined by employing the technique of X-ray diffraction (XRD). According to XRD analysis, the continuous series of $La_xCa_{1-x}MoO_{4+\delta}$ ($0 \le x \le 0.3$) solid solutions have the structure of tetragonal scheelite. Their lattice parameters are greater than that of the original sample, and increase with increasing values of x in the La-substituted system. Results of sinterability and electrochemical testing reveal that the performances of La-doped calcium molybdate are superior to that of pure $CaMoO_4$. $La_xCa_{1-x}MoO_{4+\delta}$ ceramics demonstrate higher sinterability. The $La_{0.2}Ca_{0.8}MoO_{4+\delta}$ sample that achieved 96.5% of the theoretical density was obtained after being sintered at 1250 °C for 4 h. The conductivity increases with increasing lanthanum content, and a total conductivity of 7.3×10^{-3} S cm^{-1} at 800 °C could be obtained in the $La_{0.2}Ca_{0.8}MoO_{4+\delta}$ compound sintered at 1250 °C for 4 h.

1. Introduction

Solid oxide fuel cells (SOFCs) have attracted increasing interest for their high-energy conversion efficiency, silent operation and low levels of environmental pollution. Great progress in the research and development of SOFCs has been made recently [1–5]. Traditional electrolyte based on yttria-stabilized zirconia (YSZ) is one of the most well-known electrolyte materials used for SOFCs. However, their high operating temperature (above 1000 °C) results in both high costs and system degradation at the interface between cell components [6,7]. Electrolyte materials proposed to substitute for the YSZ types of electrolytes have attracted considerable attention throughout the world.

ABO_4 scheelite-type materials have been studied in recent years. These scheelite-type oxides exhibit a high oxide ion conduction in the intermediate-temperature range, e.g., $Pb_{0.9}Sm_{0.1}WO_{4+\delta}$ shows a conductivity of 2×10^{-2} S cm^{-1} at 800 °C [8], which is comparable to that of YSZ electrolytes (3.6×10^{-2} S cm^{-1} at 800 °C). A wide variety of properties for compounds with the scheelite structure, especially electrical conduction of various substituted scheelite-type samples, have thus far been explored [8–12]. Presently, materials in solid-state devices such as electrodes and electrolytes have stimulated considerable interest in the possible applications of these materials. Scheelite-type $CaMoO_4$ has attracted interest because of its potential applications, such as electro-optical and laser host materials [13,14]. It can be easily doped with rare-earth ions, and the doped crystal can be used as an important functional material. Electrical, thermal, luminescence and reflectivity properties were studied [9,15–17], which provide a basis for our understanding of this kind of material.

Scheelite-type materials are often prepared by conventional solid-state reactions, lower temperature reactions that employing hydrothermal, precipitation, microwave irradiation and soft chemical processes [18–21]. Based on its low processing temperatures, the sol–gel method offers a new way to reduce sintering temperatures. This method has the advantages of a short reaction time, and it is simple more efficient than other conventional methods. Moreover, high purity products with small particle sizes and narrow particle size distributions can be obtained from the sol–gel process.

In the present study, the $La_xCa_{1-x}MoO_{4+\delta}$ powders were prepared by the sol–gel process. Their phase information and sinterability were investigated. Additionally, the electrochemical properties of $La_xCa_{1-x}MoO_{4+\delta}$ sintered samples were characterized to estimate if they could serve as an alternative electrolyte for SOFCs.

2. Experimental

2.1. Sample preparation

Powdered samples with the general formula of $La_xCa_{1-x}MoO_{4+\delta}$ (x = 0–0.3) were synthesized by the sol–gel process (Fig. 1). Analytically pure $La(NO_3)_3$, $Ca(NO_3)_2$ and MoO_3 were used as starting materials. $La(NO_3)_3$ and $Ca(NO_3)_2$ were dissolved into deionized water; MoO_3 was dissolved into ammonia. The two liquids were

* Corresponding author: Tel.: +86 551 2158438; fax: +86 551 2158436.
E-mail address: cjh@hfuu.edu.cn (J. Cheng).

0378-7753/$ – see front matter © 2009 Elsevier B.V. All rights reserved.
doi:10.1016/j.jpowsour.2009.10.017

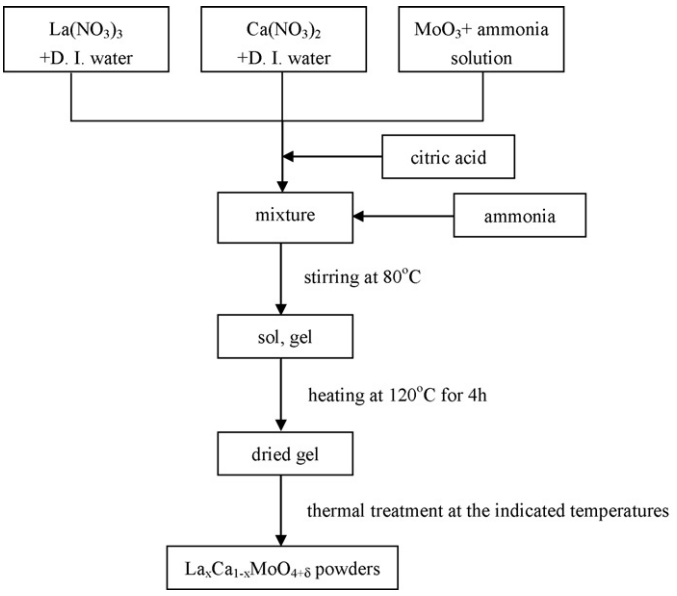

Fig. 1. Flow chart of preparing $La_xCa_{1-x}MoO_{4+\delta}$ powders by a sol–gel process.

mixed together under continuous stirring at 80 °C. Citric acid was subsequently added as a chelating and a reducing agent. The pH value of the final solution was adjusted to the desired value (approximately 7–8) by adding $NH_3{\cdot}H_2O$ in order to achieve the complete complexation of citric acid with metallic ions without precipitation. A homogeneous sol formed. The sol was heated and stirred at 80 °C to form the gel complexes. The gel was placed in an oven at 120 °C for 24 h to dry. Powders were prepared by calcining the dried gel at different temperatures for 3 h. The powders were pressed into pellets of 10 mm in diameter and 1–2 mm in thickness under 200 MPa of pressure using a 10% polyvinyl alcohol (PVA) solution as the binder. Finally, the pellets were sintered at different temperatures in an atmosphere of air for 4 h.

2.2. Characterization

Differential thermal analysis (DTA) was performed in air from 50 to 800 °C at 10 °C min^{-1}. Phase formation of the calcined oxide powders was determined by X-ray diffraction (XRD) analysis with the Cu Kα line (λ = 0.15406 nm), at angles ranging from 10° to 80°. For conductivity measurements, silver paste was painted onto both sides of the pellet samples. The samples were then fired at 500 °C for 1 h to burn out the organic binder and form Ag electrodes. The measurement of AC impedance was performed in air with an electrochemical workstation, CHI660B. The frequency range varied from 0.1 Hz to 100 kHz with an ac signal amplitude of 5 mV. Measurement of the data was conducted in the temperature range of 500–800 °C at an interval of 50 °C.

3. Results and discussion

3.1. DTA analyses

Differential thermal analysis (DTA) of the dried gel was performed in order to study the decomposition and crystallization of the precursor. The DTA plot for the $La_{0.2}Ca_{0.8}MoO_{4+\delta}$ sample is shown in Fig. 2. As seen in this figure, one endothermic peak and three exothermic peaks are observed at 60–120, 145.6, 166 and 498 °C, respectively. The endothermic peak at 60–120 °C primarily resulted from evaporation of physically adsorbed water and the removal of residual organic solvents in the dried gel.

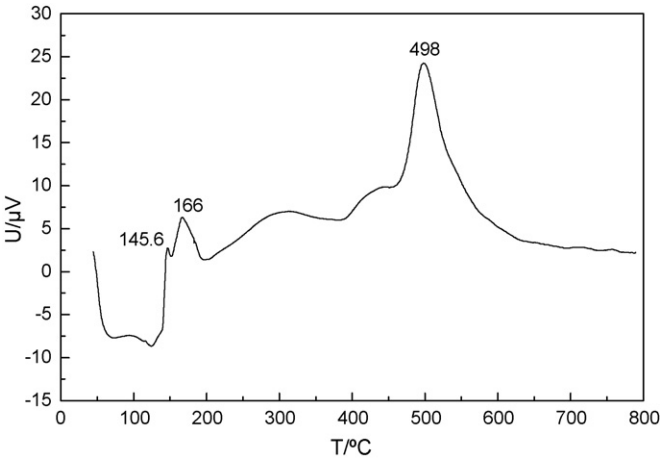

Fig. 2. DTA curve of $La_{0.2}Ca_{0.8}MoO_{4+\delta}$ from 50 to 800 °C in air.

The exothermic peaks at 145.6 and 166 °C corresponded to the decomposition and combustion of citric acid. The exothermic peak appearing at 498 °C indicated that decomposition or oxidation reactions occurred strongly at this temperature. The other exothermic peaks, at 305 and 440 °C, are attributed to the pyrolysis of nitrates in the precursor. The observations of these phenomena support the conclusion based on DTA analysis that the content of carbon and hydrogen in the precursor were decomposed completely below 500 °C.

3.2. Phase information

The XRD patterns of the $La_xCa_{1-x}MoO_{4+\delta}$ powders calcined at 900 °C for 3 h are illustrated in Fig. 3. All diffraction peaks matched well with the JCPDS file no. 85-1267. No additional diffraction peaks were found, indicating that the substitution of the La^{3+} ion at the Ca^{2+} site had occurred. The dopant La^{3+} ions were dissolved completely in the crystal lattice of $CaMoO_4$, and formed a solid solution with the general formula of $La_xCa_{1-x}MoO_{4+\delta}$ composed of a single tetragonal scheelite phase.

The tetragonal scheelite-type $La_xCa_{1-x}MoO_{4+\delta}$ solid solution extended up to $x = 0.3$ in this system, which is comparable to that in previous reports [22]. In this composition range, a shift in the

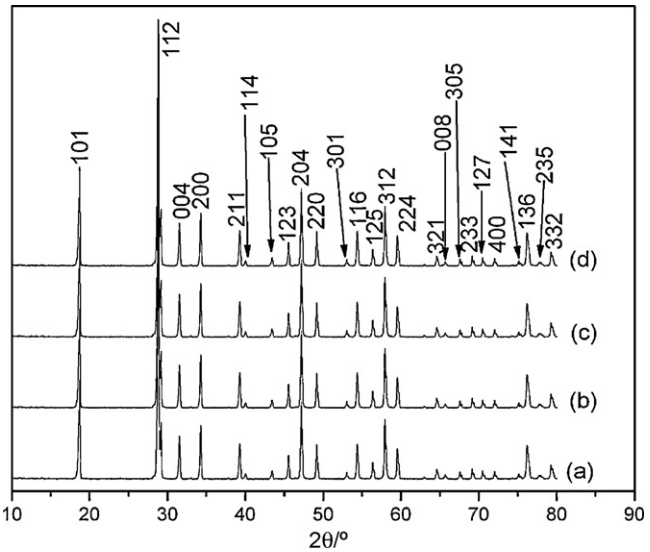

Fig. 3. X-ray diffraction patterns of $La_xCa_{1-x}MoO_{4+\delta}$ samples: (a) $x = 0$, (b) $x = 0.1$, (c) $x = 0.2$, and (d) $x = 0.3$.

Table 1
Lattice constants of $La_xCa_{1-x}MoO_{4+\delta}$ samples prepared by sol–gel process.

x value	Lattice constant (nm)		The unit cells' volume (nm^3)	Theoretical density ($g\,cm^{-3}$)	Sintered density ($g\,cm^{-3}$)
	a	c			
$x=0$	0.5223	1.1439	0.3121[a]	4.259[a]	
$x=0.1$	0.5343	1.1648	0.3317	4.469	4.325
$x=0.2$	0.5451	1.1736	0.3487	4.680	4.516
$x=0.3$	0.5557	1.1954	0.3691	4.891	4.710

[a] Unit cell volume and theoretical density evaluated from the tetragonal scheelite-type structure of $CaMoO_4$ (JCPDS file no. 85-1267).

peak position is not obvious; however, the lattice parameter of the tetragonal phase is changed and the anion lattice is distorted by the lanthanum content due to the size differences between La^{3+} and Ca^{2+}. Table 1 lists the lattice parameters of all of the scheelite electrolytes investigated. As seen in Table 1, the lattice parameters and the volumes of the unit cells increased with increasing values of x in the La-substituted system. This observation can be explained by considering the substitution for Ca^{2+} by the trivalent La^{3+} cation that has a large ionic radius.

3.3. Sintering behaviors

Fig. 4 illustrates the shrinkage curves of the $La_xCa_{1-x}MoO_{4+\delta}$ samples. The shrinkage of pure $CaMoO_4$ occurred over a broad temperature range 700–1300 °C, and the final shrinkage was less than 12%. The onset of $La_xCa_{1-x}MoO_{4+\delta}$ shrinkage occurred at lower temperature and rapid shrinkage occurred over a narrow temperature region (600–800 °C). Final shrinkage was approximately 15%, 14% and 13% for $La_{0.1}Ca_{0.9}MoO_{4+\delta}$, $La_{0.2}Ca_{0.8}MoO_{4+\delta}$ and $La_{0.3}Ca_{0.7}MoO_{4+\delta}$, respectively. Shrinkage differences can be attributed to the size differences between La^{3+} and Ca^{2+} and differences in lanthanum content.

The relative density of the sintered ceramic samples was measured using the standard Archimedes method. Fig. 5 shows the relative density of $La_xCa_{1-x}MoO_{4+\delta}$ ceramics sintered at various temperatures. As seen in Fig. 5, the density of sintered $La_xCa_{1-x}MoO_{4+\delta}$ ceramics increased with temperature and reached a density of 96.5% of the theoretical value when sintered at 1250 °C for 4 h. When the sintering temperature is greater than

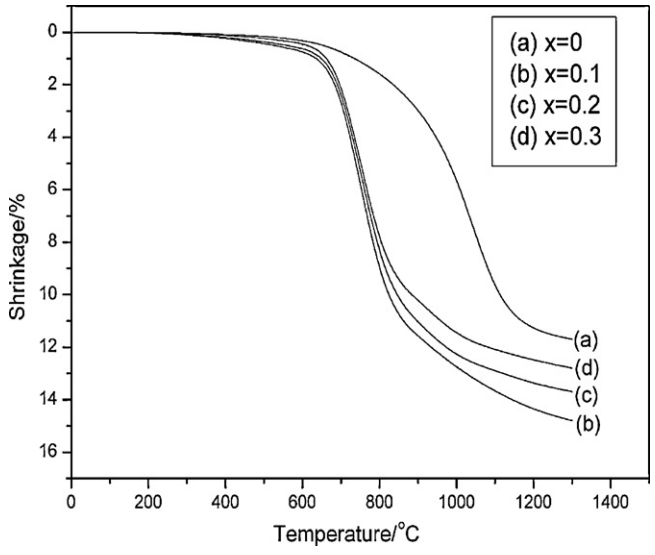

Fig. 4. Shrinkage curves of $La_xCa_{1-x}MoO_{4+\delta}$ samples as a function of sintering temperature.

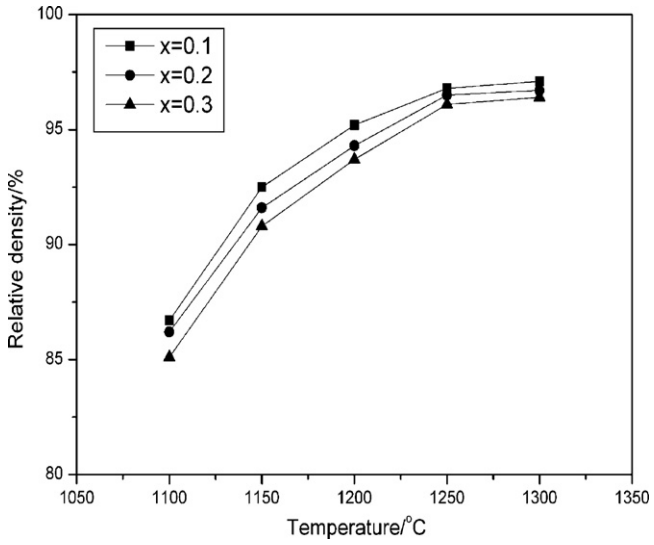

Fig. 5. Dependence of relative density on sintering temperatures for $La_xCa_{1-x}MoO_{4+\delta}$ ceramics.

1250 °C, the density of sintered ceramics did not improve. Therefore, the ideal sintering temperature of $La_xCa_{1-x}MoO_{4+\delta}$ ceramics is 1250 °C, which is considerably lower than that of other fluorite or perovskite-type electrolytes [23–25]. Conversely, the relative density of $La_xCa_{1-x}MoO_{4+\delta}$ sintered ceramics decreases on a small scale with increasing values of x, which can be understood by considering the substitution of different cation sizes.

Fig. 6 exhibits a cross-sectional view of the $La_{0.2}Ca_{0.8}MoO_{4+\delta}$ electrolyte sintered at 1250 °C for 4 h. The electrolyte pellet is quite dense and uniform; the cross-sectional view is void of any obvious pores and cracks, which indicates good sintering.

3.4. Electrical conductivity

Fig. 7 shows typical impedance plots for $La_{0.2}Ca_{0.8}MoO_{4+\delta}$ sintered pellets measured in air at various temperatures. A single semicircle was observed and the low frequency intercept is measured for evaluation of the conductivity data. The impedance

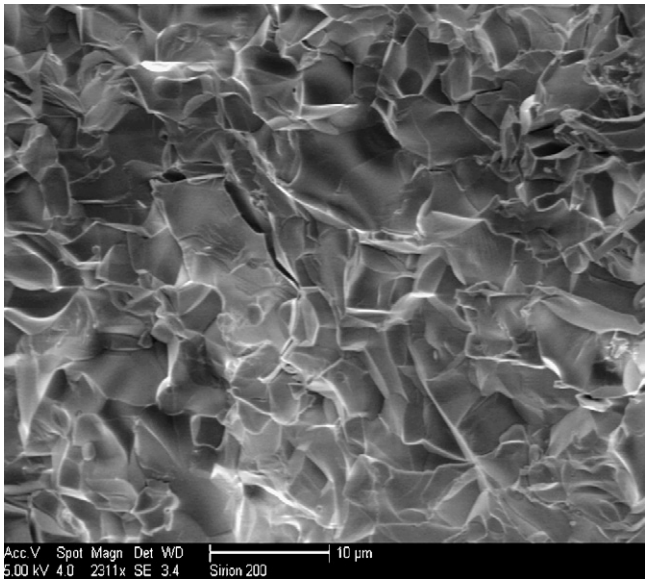

Fig. 6. Cross-section of $La_{0.2}Ca_{0.8}MoO_{4+\delta}$ electrolyte sintered at 1250 °C for 4 h.

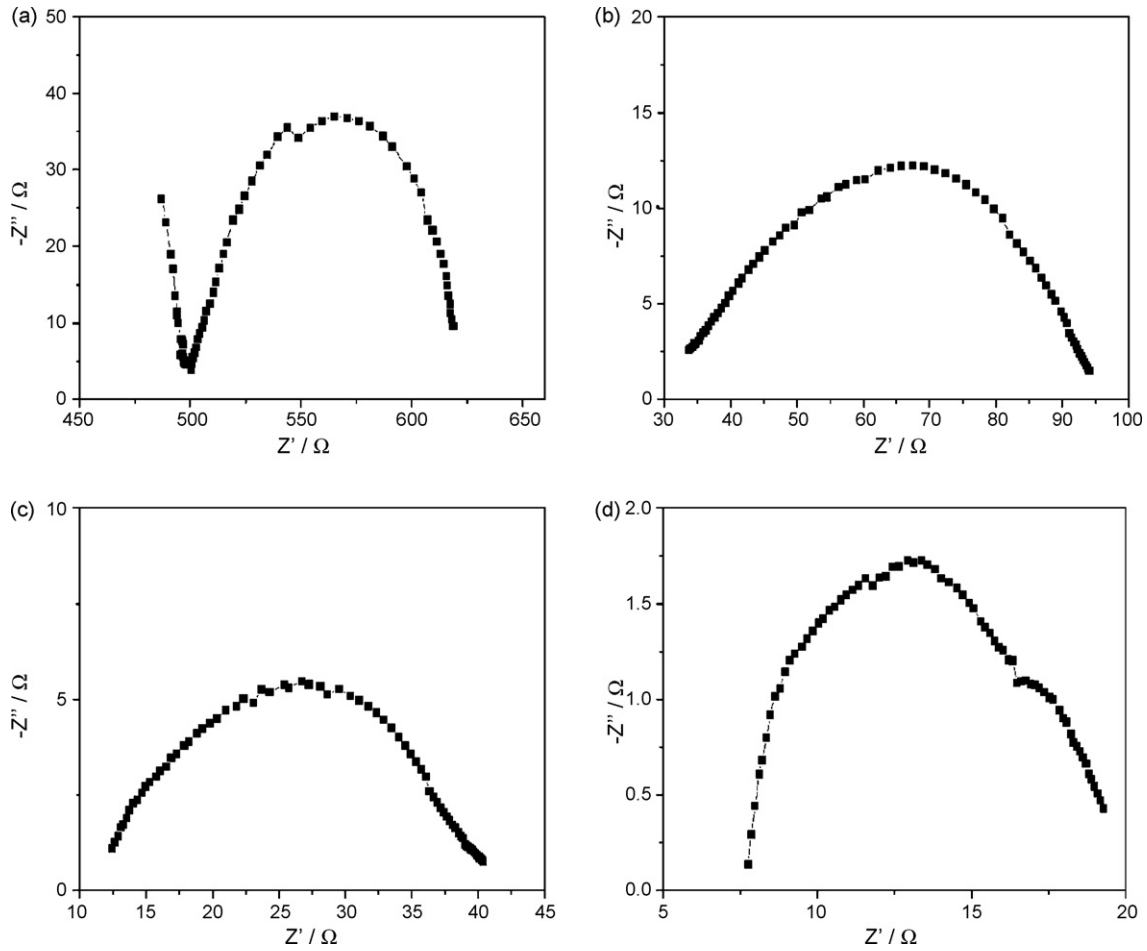

Fig. 7. Impedance spectra of $La_{0.2}Ca_{0.8}MoO_{4+\delta}$ tested at: (a) 500 °C, (b) 600 °C, (c) 700 °C, (d) 800 °C.

spectral data were fitted with a suitable equivalent circuit of the zsimpwin software to distinguish the bulk resistance and grain-boundary resistance, and calculate the conductivities. The total resistance of the electrolyte can be expressed as:

$$R_t = R_b + R_{gb} \quad (1)$$

where R_b is the bulk resistance and R_{gb} is the grain-boundary resistance. Therefore, the total resistance of the electrolyte can be obtained from the spectrum and converted to a conductivity datum σ, using the relationship:

$$\sigma = \frac{L}{R \cdot S} \quad (2)$$

where L is the sample thickness and S is the electrode area on the sample surface. These parameters are compiled in Table 2. As the operating temperature increased, the total resistance decreased, and the electrical conductivity datum increased. The conductivity of $La_{0.2}Ca_{0.8}MoO_{4+\delta}$ sintered at 1250 °C for 4 h in air reached 7.3×10^{-3} S cm^{-1} at 800 °C. This value is near to that of other perovskite, apatite or fluorite-type electrolytes, which have been studied in-depth for SOFCs [6,26], indicating that lanthanum-doped $CaMoO_4$ is a promising electrolyte for intermediate-temperature SOFCs.

Representative Arrhenius plots of conductivity measured in air are shown in Fig. 8. Enhanced conductivities are observed in the samples in which lanthanum is substituted. For pure $CaMoO_4$, the conductivity is 5.0×10^{-5} S cm^{-1} at 800 °C [27]. The conductivity increased gradually with increasing lanthanum content within the solubility range. However, when the lanthanum content exceeded 20%, the conductivity decreased. Analogous results were observed in the La-substituted system as well as in CeO_2-based fluorite-type phases [28–30]. In our study, the partial substitution of La with Ca might cause two opposite effects. The ordering of the oxygen vacancy might be suppressed, which led to the decrease in activation energy of conduction and an increase in ionic conductivity

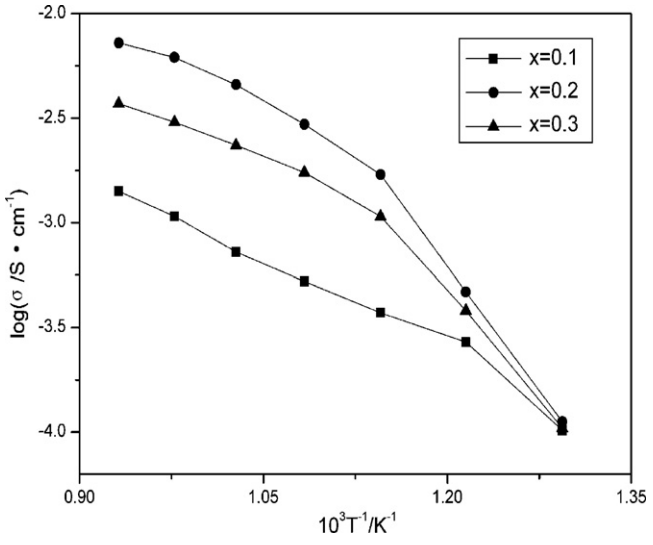

Fig. 8. Arrhenius plot comparing the total electric conductivity of $La_xCa_{1-x}MoO_{4+\delta}$.

Table 2
Total resistance and electrical conductivity of $La_{0.2}Ca_{0.8}MoO_{4+\delta}$ at various temperatures.

	T (°C)						
	500	550	600	650	700	750	800
R (Ω)	500.3	121.1	33.7	19.1	12.5	9.3	7.8
σ (S cm^{-1})	1.13×10^{-4}	4.68×10^{-4}	1.68×10^{-3}	2.96×10^{-3}	4.54×10^{-3}	6.12×10^{-3}	7.30×10^{-3}

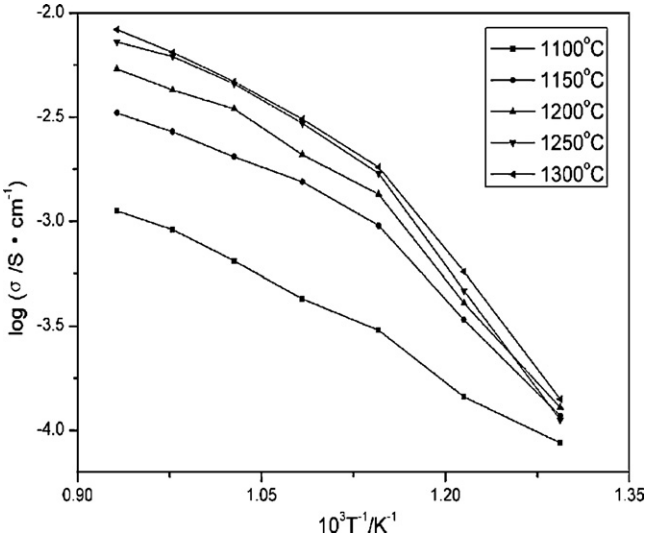

Fig. 9. Dependence of the conductivity on temperature for $La_{0.2}Ca_{0.8}MoO_{4+\delta}$ ceramic.

[31]. Additionally, the deviation of the lattice parameter from that of pure $CaMoO_4$ was enlarged, as shown in Table 1, which led to the increase in the activation energy of conduction and the decrease in ionic conductivity. Therefore, the electrolyte with the greater ionic conductivity must contain an appropriate dopant concentration. For the $La_xCa_{1-x}MoO_{4+\delta}$ samples, the greatest conductivity was observed in the $x = 0.2$ sample.

The high-frequency limit in this study was 100 kHz which is the upper limit for the electrochemical workstation (CHI660B) used. This frequency is insufficient and resulted in an incomplete semicircle, which makes it difficult to determine the grain resistance and the grain-boundary resistance. Although significant uncertainties exist in the electrolyte resistance estimated from the impedance data, the activation energies for $La_xCa_{1-x}MoO_{4+\delta}$ samples can be obtained from Arrhenius plots (Fig. 8). In the case in which the conductivities exhibited small interruptions at 600–650 °C, they were calculated in two temperature regions—greater than 650 °C and less than 600 °C. These temperatures demarcate the contribution to the two conductivities by the two different types of charge carriers [27]. The activation energies of the $La_{0.2}Ca_{0.8}MoO_{4+\delta}$ sample in the two temperature regions are 0.56 and 0.87 eV, respectively.

In order to investigate the effect of sintering temperature on the properties of $La_xCa_{1-x}MoO_{4+\delta}$, a series of sintering conditions were studied. Fig. 9 shows the logarithm of the electrical conductivity plotted versus the reciprocal temperature of the $La_{0.2}Ca_{0.8}MoO_{4+\delta}$ samples. The electrical conductivity datum increased as the sintering temperature increased, and reached a value of 7.3×10^{-3} S cm^{-1} at 1250 °C, which is satisfactory for SOFCs. However, when the sintering temperature exceeded 1250 °C, the conductivity did not increase. The reason may be that loss of the lattice oxygen in this system at high temperatures caused the decrease in electrical conductivity due to the reduction of charge carrier concentration [32].

4. Conclusions

The sol–gel process was used to synthesize scheelite-type electrolyte materials, of the formula $La_xCa_{1-x}MoO_{4+\delta}$ in which $x = 0$–0.3. The phase formation, sintering behaviors and electrochemical properties of these compounds were investigated. The results indicated that, when doped with trivalent La^{3+} cations, the scheelite lattice of $CaMoO_4$ expanded. $La_xCa_{1-x}MoO_{4+\delta}$ samples show higher sinterability than pure $CaMoO_4$, and the $La_xCa_{1-x}MoO_{4+\delta}$ sample achieved 96.5% of the theoretical density after being sintered at 1250 °C for 4 h. The total conductivity value peaked at $x = 0.2$ in the temperature range of 500–800 °C for La-doped $CaMoO_4$ electrolyte materials.

Acknowledgement

This work was kindly supported by the Natural Science Foundation of Education Department of Anhui Province under contract no. KJ2009B045Z.

References

[1] Y.C. Liou, S.L. Yang, J. Power Sources 179 (2008) 553–559.
[2] F. Baratto, U.M. Diwekar, J. Power Sources 139 (2005) 188–196.
[3] G.Y. Meng, G.L. Ma, Q.L. Ma, R.R. Peng, X.Q. Liu, Solid State Ionics 178 (2007) 697–703.
[4] Y. Matsuzaki, Y. Baba, T. Sakurai, Solid State Ionics 174 (2004) 81–86.
[5] K. Xie, R.Q. Yan, X.R. Chen, D.H. Dong, S.L. Wang, X.Q. Liu, G.Y. Meng, J. Alloys Compd. 472 (2009) 551–555.
[6] D. Lee, J.H. Han, Y. Chun, R.H. Song, D.R. Shin, J. Power Sources 166 (2007) 35–40.
[7] B. Huang, X.J. Zhu, W.Q. Hu, Q.C. Yu, H.Y. Tu, J. Power Sources 186 (2009) 29–36.
[8] T. Esaka, Solid State Ionics 136–137 (2000) 1–9.
[9] V. Thangadurai, C. Knittlmayer, W. Weppner, Mater. Sci. Eng. B 106 (2004) 228–233.
[10] T. Tojo, Q. Zhang, F. Saito, J. Alloys Compd. 427 (2007) 219–222.
[11] M.A.M.A. Maurera, A.G. Souza, L.E.B. Soledade, F.M. Pontes, E. Longo, E.R. Leite, J.A. Varela, Mater. Lett. 58 (2004) 727–732.
[12] E.V. Tsipis, C.N. Munnings, V.V. Kharton, S.J. Skinner, J.R. Frade, Solid State Ionics 177 (2006) 1015–1020.
[13] C.H. Cui, J. Bi, D.J. Gao, Mater. Lett. 62 (2008) 2222–2224.
[14] T.Y. Liu, J. Chen, F.N. Yan, J. Lumin. 129 (2009) 101–104.
[15] N. Sharma, K.M. Shaju, G.V. Subba Rao, B.V.R. Chowdari, Z.L. Dong, T.J. White, Chem. Mater. 16 (2004) 504–512.
[16] N. Sharma, G.V. Subba Rao, B.V.R. Chowdari, Electrochim. Acta 50 (2005) 5305–5312.
[17] N. Sharma, K.M. Shaju, G.V. Subba Rao, B.V.R. Chowdari, Electrochem. Commun. 4 (2002) 947–952.
[18] A. Phuruangrat, T. Thongtem, S. Thongtem, J. Alloys Compd. 481 (2009) 568–572.
[19] G.K. Choi, S.Y. Cho, J.S. An, K.S. Hong, J. Eur. Ceram. Soc. 26 (2006) 2011–2015.
[20] Y. Wang, J. Ma, J. Tao, X. Zhu, J. Zhou, Z. Zhao, L. Xie, H. Tian, Ceram. Int. 33 (2007) 693–695.
[21] F. Lei, B. Yan, J. Solid State Chem. 181 (2008) 855–862.
[22] T. Esaka, R. Tachibana, S. Takai, Solid State Ionics 92 (1996) 129–133.
[23] Q. Wang, R. Peng, C. Xia, W. Zhu, H. Wang, Ceram. Int. 34 (2008) 1773–1778.
[24] Z. Zhong, Solid State Ionics 178 (2007) 213–220.
[25] M. Han, X. Tang, H. Yin, S. Peng, J. Power Sources 165 (2007) 757–763.
[26] S.W. Zha, C.R. Xia, G.Y. Meng, J. Power Sources 115 (2003) 44–48.
[27] S.K. Arora, R.S. Godbole, D. Lakshminarayana, J. Mater. Sci. 18 (1983) 1359–1364.
[28] H. Iwahara, T. Esaka, T. Sato, T. Takahashi, J. Solid State Chem. 39 (1981) 173–180.
[29] H. Yamamura, E. Katoh, M. Ichikawa, K. Kakinuma, T. Mori, H. Haneda, Electrochemistry 68 (2000) 455–459.
[30] X. Sha, Z. Lv, X. Huang, J. Miao, Z. Ding, X. Xin, W. Su, J. Alloys Compd. 428 (2007) 59–64.
[31] H. Inaba, H. Tagawa, Solid State Ionics 83 (1996) 1–16.
[32] H. Zhao, D. Teng, X. Zhang, C. Zhang, X. Li, J. Power Sources 186 (2009) 305–310.